A Comparison Between Different Propagative Schemes for the Simulation of Tapered Step Index Slab Waveguides

Jan Haes, Roel Baets, *Member, IEEE,* C. M. Weinert, M. Gravert, H. P. Nolting, M. Adelaide Andrade, A. Leite, Hans K. Bissessur, J. B. Davies, Robert D. Ettinger, Jiri Ctyroky, E. Ducloux, F. Ratovelomanana, N. Vodjdani, Stefan Helfert, Reinhold Pregla, *Senior Member, IEEE,* F. H. G. M. Wijnands, H. J. W. M. Hoekstra, and G. J. M. Krijnen

Abstract—The performance and accuracy of a number of propagative algorithms are compared for the simulation of tapered high contrast step index slab waveguides. The considered methods include paraxial as well as nonparaxial formulations of optical field propagation. In particular attention is paid to the validity of the paraxial approximation. To test the internal consistency of the various methods the property of reciprocity is verified and it is shown that for the paraxial algorithms the reciprocity can only be fulfilled if the paraxial approximation of the power flux expression using the Poynting vector is considered. Finally, modeling results are compared with measured fiber coupling losses for an experimentally realized taper structure.

I. INTRODUCTION

THE REALIZATION of cost effective and highly performant laser diode or III-V semiconductor optical waveguide to single mode fiber coupling arrangements is a major research topic in optoelectronics. The rectangular laser geometry and the circular shape of the fiber in combination with the discrepancy in refractive index contrast between core and cladding (5–10% compared to about 0.5% for laser and fiber respectively), leads to an order of magnitude difference in laser and fiber spot size. Hence, direct butt coupling between laser and fiber leads to intolerable insertion losses of typical 10 dB. Matching both spot sizes to each other reduces the coupling loss. This can be done using lensed fibers whether

or not in combination with a spot size transforming element acting directly on the laser beam. Microlens systems are conventionally used for this purpose. The resulting packaging cost is large for these nonintegrated mode expansion optics. A more attractive approach consists of integrating a spot size transformer with the laser waveguide. An example of an integrated mode adapter is a tapered waveguide.

The experimental realization of tapered waveguides and lasers has been reported quite extensively in the literature for the last few years, see for example [1]. The technological processes involved require complicated growth techniques, like shadow mask growth or selective growth, or difficult etching processes, e.g., dynamic etching or diffusion limited etching. It is therefore important to have an accurate and powerful modeling tool or design criterion able to predict the influence of different geometrical parameters on the performance of the taper. Due to the gradual change of the refractive index profile in the propagation direction there is a continuous power transfer between the guided mode and the radiation field, unless the taper is (almost) adiabatic. A simple design criterion for adiabatic tapering is readily available [2]. A more detailed analysis is possible by for example the coupled mode theory, which is commonly used for the analysis of grating devices, but is sometimes cumbersome when applied to tapered devices [3]. The beam propagation method (BPM) on the other hand is widely used to model various kinds of waveguides. More complicated adiabaticity criteria require a propagative analysis anyway [4].

In this paper we address the applicability of different propagative schemes in the case of tapered high contrast step index slab waveguides, i.e., only one transverse dimension and the propagation direction are taken into account. The waveguides under consideration have index profiles which may be regarded as typical for the vertical cross section of state of the art tapers. As long as, in the three dimensional taper, the horizontal guiding structure and spot size are relatively broad over the whole taper length, the modeling of the vertical cross section only is able to predict accurately the vertical beam properties [5].

The presented work was done in the framework of the COST 240 project "Techniques of Modeling and Measuring Advanced Photonic Telecommunication Components." Eight

TABLE 1

OVERVIEW OF ALL PARTICIPANTS IN THE MODELING EXERCISE AND DETAILS OF THE IMPLEMENTED METHODS. THE 5th COLUMN LISTS THE CHOICE OF
REFERENCE INDEX FOR THE PARAXIAL METHODS. THE UNIVERSITY OF TWENTE USED $n_0 = 3.18$ IN THE SEMI CASE AND $n_0 = 3.20$ IN THE
AIR CASE. WHEN $n_0 = n_{eff,in}$, THE EFFECTIVE INDEX (UP TO TWO DIGITS AFTER THE FLOATING POINT) OF THE LOCAL FUNDAMENTAL
MODE AT THE WAVEGUIDE INPUT SIDE IS TAKEN AS A REFERENCE. THE ($\times$) SYMBOL INDICATES INCOMPLETE TM RESULTS

Participant	Equation	Numerical method	Boundary condition (BC)	Reference index	Polarisation TE	TM
Univ Twente	Fresnel	FD-BPM	Transparent	3.18 / 3.20	x	x
Univ Porto		FD-BPM	Transparent	Eq. (1)	x	(x)
HHI		FD-BPM	Absorber	Eq. (1)	x	
Thomson-CSF		FD-BPM	Transparent	n_{cl}	x	x
AAR-UCL		FE-BPM	Window functions	$n_{eff,in}$	x	x
Univ Hagen	Helmholtz	MoL-BPM	Absorbing BC	-	x	x
IREE Prague		MEPM	Absorber	-	x	x
Univ Gent		MEPM	Window functions	-	x	x

SEMI   AIR
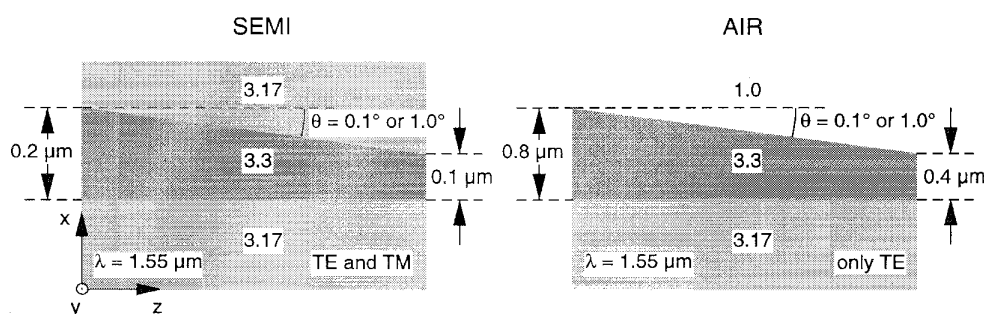

Fig. 1.   Schematic view of the SEMI and AIR tapers.

different laboratories participated. The simulations cover both paraxial and nonparaxial propagation, finite difference methods and eigenmode expansion techniques. For a number of linear tapers with different index contrast and opening angle, the calculated power loss of the fundamental mode is compared. To test the internal consistency of the different propagation schemes, the reciprocity of the propagation is verified. In order to allow for comparison between simulation and experiment the fiber butt coupling losses of a taper structure fabricated and characterized by the Heinrich Hertz Institute is calculated.

II. OVERVIEW OF THE PROPAGATION METHODS

From eight different contributions, there were five algorithms based on the paraxial approximation and three nonparaxial algorithms, relying on modal expansion techniques. Hence, it will be possible to address the problem of the validity of the paraxial approximation for the modeling of tapered high contrast step index waveguides. An overview of the participating institutions and implemented methods is listed in Table I.

A. Paraxial Algorithms

All paraxial algorithms are finite difference methods (FD-BPM) that solve the scalar Fresnel wave equation for the dominant field component (E_y for TE polarization or H_y for TM, the coordinate system is defined in Fig. 1). The only exception is the finite element (FE-BPM) method of Alcatel

Alsthom Research-University College London (AAR-UCL), which accounts for the full vectorial components of the magnetic **H** field. Fresnel's wave equation follows from the Helmholtz equation (see Section II-B) by introducing a reference propagation factor $\exp(-j\beta_0 z)$, with β_0 the reference propagation constant, and by making the slowly varying envelope approximation (SVEA). All algorithms use direct Crank–Nicolson discretization of the paraxial wave equation [6]; no split step finite difference schemes [7], which are usually applied in the three dimensional case, are considered. Hadley's transparent boundary conditions are applied [8] in most cases.

The University of Twente implements the SVEA with higher order corrections using a perturbation technique [9], [10]. In this way the differences between the reference propagation constant β_0 and the varying propagation constant of the local fundamental mode can be compensated at the expense of some computing time. Applying the second order correction increases for instance the computing time by almost a factor of two. One might argue that the inclusion of the higher order correction terms in the algorithm results in a nonparaxial solution.

The algorithm of the University of Porto, based on [11], uses an adaptive reference propagation constant. At each propagation step a new value of β_0 is calculated by overlapping the propagating field $\psi(x, z)$ with the local normal modes $\varphi_i(x)$

TABLE II
GEOMETRICAL PARAMETERS OF THE DIFFERENT
TAPER STRUCTURES SEMI AND AIR OF FIG. 1

	Input thickness [μm]	Output thickness [μm]	Opening angle θ [°]	Length L [μm]
SEMI	0.2	0.1	0.1	57.3
			1.0	5.73
AIR	0.8	0.4	0.1	229
			1.0	22.9

of the waveguide [12]

$$\beta_0^2 = \frac{\sum_i \beta_i^2 \left| \int \psi(x, z)\varphi_i(x)dx \right|^2}{\sum_i \left| \int \psi(x, z)\varphi_i(x)dx \right|^2}. \tag{1}$$

Incorporating this technique into a standard BPM algorithm introduces some mode expansion (see Section II-B) aspects into the calculation. In this way, a kind of hybrid formulation of the BPM is obtained. The algorithm of Heinrich Hertz Institute uses a similar adaptive reference propagation constant.

Thomson-CSF has implemented the standard finite difference BPM without any correction for the reference propagation constant.

The three dimensional algorithm of Alcatel Alsthom Research-University College London is based on a vectorial H field formulation [13] because the magnetic field is continuous across the boundaries in dielectric media. For the two dimensional taper simulations, arbitrary electric or magnetic walls were introduced to reduce the problem by one dimension. A finite element based discretization scheme is used in the transverse dimensions and a Crank–Nicolson finite difference discretization in the propagation direction. The mesh was chosen linear in the guide and logarithmic in the cladding layers.

B. Nonparaxial Algorithms

The nonparaxial approximation solves the scalar Helmholtz equation for the dominant field component. As long as piecewise constant refractive index profiles are considered and the correct boundary conditions for the different field components are taken into account, this equation describes exactly the field propagation for both TE and TM polarizations. The basic approximation made is therefore the discretization of the continuous taper profile into a staircase refractive index distribution. Different discretization efforts will be considered to address this problem.

It is seen in Table II that two different algorithms were used: the Method of Lines BPM (MoL–BPM) and the mode expansion propagation method (MEPM). The MoL-BPM was implemented by the University of Hagen; the MEPM by the IREE Prague and the University of Gent.

The MoL–BPM is an eigenmode propagation algorithm which solves directly the Helmholtz equation. The full wave equation is solved analytically on lines in the propagation direction and discretised in the transverse directions using finite differences. There are no restrictions on the refractive index steps. Radiation modes are taken into account using absorbing boundary conditions [14]. At discontinuities a point

matching of the tangential field components takes place by considering reflected modes [15]. Taper structures can be analyzed using a staircase approximation of the structure or by calculating in cylindrical coordinates [16], [17]. The cylindrical coordinate system has the advantage that the taper profile itself does not need to be discretized. However, since the straight waveguide sections at input and output have to be described in the Cartesian coordinate system the matching of the field profile at the interfaces between both coordinate systems complicates matters.

In the MEPM [18], [19] no discretization (the lines in the MoL–BPM) in the transverse coordinate is needed. Instead, the propagating field is decomposed into the guided modes of the waveguide and a well chosen set of radiation and evanescent modes. This corresponds to a discretization in the wavevector space. The discretization is performed by enclosing the waveguide structure in a metallic box for TE modes or a magnetic box for TM modes. The reflection of radiation modes [20] at these artificial boundaries can be eliminated by introducing an absorbing region in their neighborhood [18] or by using window functions [4]. The use of an absorber (as implemented by IREE Prague) requires a complex mode solver while in the window function approach (University of Gent) all modes have a pure real or pure imaginary propagation constant. In the implementation of the bidirectional algorithm care is taken of the noncoherent reflections only. At each vertical interface the reflection coefficients for the different modes are calculated, but the modes are not propagated backward. This approximation excludes eventual interference effects of the reflected fields. In tapered waveguides this approximation is valid, to the contrary of the case of, e.g., a grating assisted coupler device.

III. DESCRIPTION OF THE LINEAR TAPER STRUCTURES

The tapers under consideration are schematically shown in Fig. 1 and Table II summarizes the geometrical parameters of the different structures. The taper profile is linear in all cases with a pure real refractive index distribution. Two opening angles of 0.1° and 1.0° are considered and the cover is either semiconductor material (labeled SEMI) or air (labeled AIR). There is a factor of two thickness reduction between input and output section, which is practically achievable by, e.g., shadow mask growth. The taper is excited by the local fundamental mode at the input side at a wavelength of 1.55 μm and carrying unit power. All tapers are single moded. Simulations are done both for TE and TM polarization, except for the air cover case where only the TE case is considered since the waveguide does not support a guided TM mode at the output. The TE modal profiles at the different input and output sections are plotted in Fig. 2. The corresponding TM field profiles cannot be distinguished from their TE counterparts.

The power content of the local fundamental mode at half the taper length and at the output are calculated. To verify the internal consistency of the various methods the principle of reciprocity is tested. If the local fundamental mode is launched with unit power at the left side of the taper in Fig. 1, then at the output, the local fundamental mode carries a power
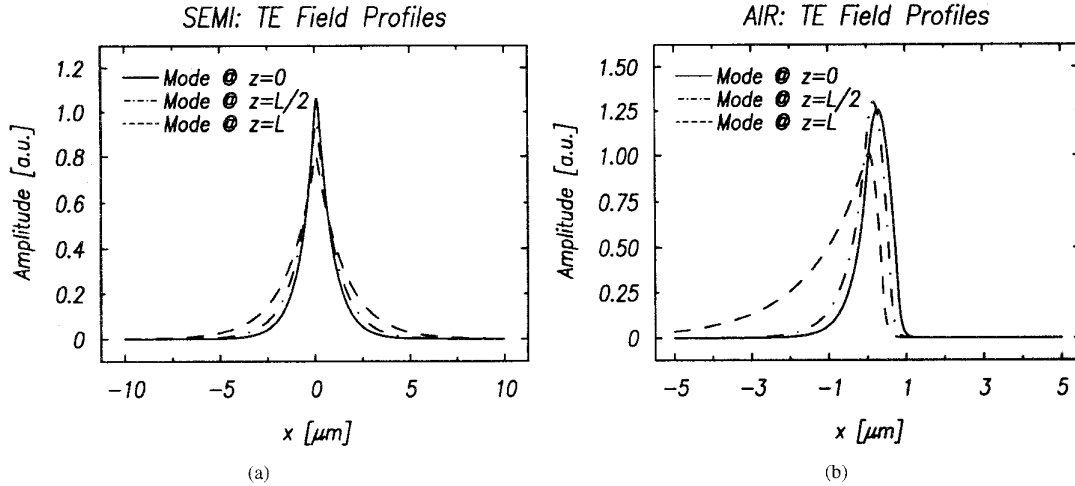
Fig. 2. TE modal field profiles at input, halfway and output cross sections of the SEMI (a) and AIR (b) tapers depicted in Fig. 1.

TABLE III
SUMMARY OF THE FUNDAMENTAL MODE POWER LOSS VALUES α AS OBTAINED BY THE DIFFERENT PARTICIPANTS FOR THE TE MODE PROPAGATION IN THE SEMI TAPERS. AN INDICATION OF THE DISCRETIZATION EFFORT IS ALSO LISTED. IN THE N_X CELL FOR AAR-UCL FIRST THE N_X-FORWARD IS GIVEN AND THEN THE N_X-BACKWARD VALUE. THE ASTERISK IN THE MEPM RESULTS DENOTE THAT N_X STANDS FOR THE NUMBER OF MODES INSTEAD OF THE TRANSVERSE DISCRETIZATION

SEMI	$\theta = 0.1°$					$\theta = 1.0°$					
TE	$L = 57.3 \ \mu m$					$L = 5.73 \ \mu m$					
	Forward		Backward			Forward		Backward			
	$\alpha(L/2)$ [%]	$\alpha(L)$ [%]	$\alpha(L/2)$ [%]	$\alpha(L)$ [%]	N_z	$\alpha(L/2)$ [%]	$\alpha(L)$ [%]	$\alpha(L/2)$ [%]	$\alpha(L)$ [%]	N_z	N_x
Twente	0.69	2.68	2.42	2.70	100	1.54	8.82	3.45	8.81	10	2048
Porto	0.70	2.69	2.42	2.70	100	1.54	8.81	3.44	8.81	10	2500
HHI	0.70	2.50	2.50	2.50	1061	1.60	8.90	3.60	8.80	106	1024
Thomson	0.69	2.72	2.42	2.73	573	1.54	8.82	3.46	8.82	57	1024
AAR-UCL	0.69	2.50	2.50	2.50	115	1.60	8.59	3.39	9.22	23	120/170
Hagen	0.70	2.72	2.42	2.72	50	1.55	8.81	3.45	8.81	50	323
IREE[*]	0.68	2.69	2.42	2.69	200	1.53	8.78	3.45	8.78	200	50
Gent[*]	0.69	2.69	2.42	2.69	20	1.53	8.82	3.44	8.82	20	51

$1 - \alpha(L)$ where $\alpha(L)$ represents the power loss of the guided mode due to the propagation through the taper structure. If one excites the same taper at the opposite side with the local fundamental mode again carrying unit power, then the power content after counter propagation will again be $1 - \alpha(L)$. The total fundamental mode power loss is therefore independent of the propagation direction. It should be stressed that reciprocity cannot give information about the power distribution at any intermediate z position.

IV. NUMERICAL RESULTS

In this section an overview of the numerical results for all simulated tapers is given. The power losses of the TE polarized fundamental mode in the SEMI case are listed in Table III. It is seen that most results agree very well with each other, leading to a calculated power loss of $\alpha(L) = 2.7\%$ for $\theta = 0.1°$ and of $\alpha(L) = 8.8\%$ for $\theta = 1.0°$. The $\alpha(L)$ results from HHI and AAR–UCL seem to give a slightly underestimated total power loss for the lower taper angle, while for the larger one a small asymmetry with respect to the reciprocity is noticed. The

field propagation for the $\theta = 0.1°$ case, forward propagation is plotted in Fig. 3. The $\theta = 1.0°$ taper is too short to be able to broaden the field profile.

Unfortunately not all participants were able to perform the TM simulations, see Table IV. From the paraxial algorithms the University of Twente, Thomson–CSF and AAR-UCL provided all results. The Twente and Thomson results are in good agreement with the MoL–BPM, using the Cartesian coordinate system, and MEPM (IREE and Gent) calculations. The Mol–BPM and AAR–UCL results show a small asymmetry in the reciprocity test. Loss figures are higher for TM propagation compared to TE propagation: $\alpha(L) = 3.4\%$ (+0.7%) for $\theta = 0.1°$ and $\alpha(L) = 9.1\%$ (+0.3%) for $\theta = 1.0°$. The result of the University of Porto ($\theta = 1.0°$, forward propagation) overestimates the power loss, while the AAR–UCL simulations show for both taper angles a small deviation from the nominal values. The different loss figures for the SEMI tapers are graphically compared in Fig. 4.

The simulations on the last example (AIR case, only TE polarization) are summarized in Table V and Fig. 5. There
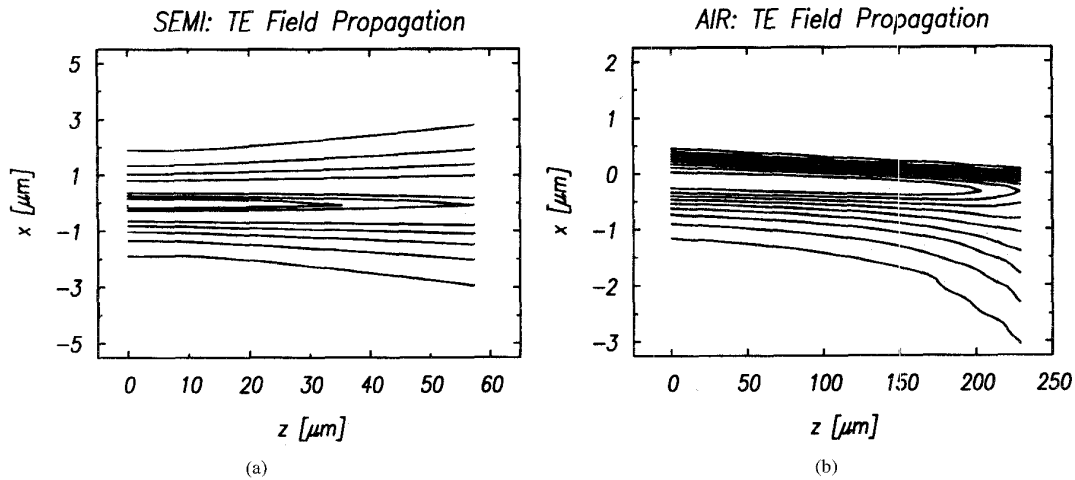
SEMI: TE Field Propagation

AIR: TE Field Propagation

(a)

(b)

Fig. 3. Contour plot of the TE field propagation for the $\theta = 0.1°$ case for the SEMI (a) and AIR (b) tapers. The propagation direction is in both cases the forward direction. The plots were obtained by the Gent–MEPM using 50 propagation steps and 51 modes for the SEMI case and 60 modes for the AIR case. The waveguide/air interface is clearly visible.

TABLE IV

SUMMARY OF THE FUNDAMENTAL MODE POWER LOSS VALUES α AS OBTAINED BY THE DIFFERENT PARTICIPANTS FOR THE TM MODE PROPAGATION IN THE SEMI TAPERS. AN INDICATION OF THE DISCRETIZATION EFFORT IS ALSO LISTED. IN THE N_X CELL FOR AAR-UCL FIRST THE N_X-FORWARD IS LISTED AND THEN THE N_X-BACKWARD VALUE. THE ASTERISK IN THE MEPM RESULTS DENOTE THAT N_X STANDS FOR THE NUMBER OF THE MODES INSTEAD OF THE TRANSVERSE DISCRETIZATION

SEMI TM	$\theta = 0.1°$ $L = 57.3$ μm					$\theta = 1.0°$ $L = 5.73$ μm					
	Forward		Backward			Forward		Backward			
	$\alpha(L/2)$ [%]	$\alpha(L)$ [%]	$\alpha(L/2)$ [%]	$\alpha(L)$ [%]	N_z	$\alpha(L/2)$ [%]	$\alpha(L)$ [%]	$\alpha(L/2)$ [%]	$\alpha(L)$ [%]	N_z	N_x
Twente	0.82	3.37	2.64	3.40	100	1.61	9.15	3.53	9.14	10	2048
Porto	-	-	-	-	-	1.95	9.70	-	-	10	2500
Thomson	0.81	3.39	2.64	3.40	573	1.59	9.13	3.53	9.15	57	1024
AAR-UCL	0.78	3.17	2.73	3.17	115	1.60	9.43	3.62	9.64	23	120/170
Hagen	0.81	3.39	2.69	3.45	50	1.60	9.15	3.58	9.20	50	324
IREE*	0.81	3.37	2.63	3.37	200	1.59	9.10	3.52	9.10	200	50
Gent*	0.82	3.37	2.63	3.37	20	1.60	9.13	3.52	9.13	20	51

is again a good agreement between the different modeling methods, although the mutual variations are somewhat larger than for the SEMI case. The modal power losses are $\alpha(L) = 3.4\%$ for $\theta = 0.1°$ and $\alpha(L) = 17.8\%$ for $\theta = 1.0°$. For $\theta = 0.1°$, the paraxial algorithms are not able to fulfil the reciprocity criterion exactly. The loss figures of HHI and Hagen, using the cylindrical coordinate system, seem to give an upper limit for the power losses. The field evolution for $\theta = 0.1°$ is drawn in Fig. 3.

V. DISCUSSION

A. Applicability of Paraxial Algorithms

It was clear from the description of the paraxial methods in Section III that some algorithms take care extensively of the choice of the reference propagation constant β_0; the algorithm of the University of Porto allows for example explicitly for a z dependent β_0 [see (1)]. In a down tapered waveguide the local fundamental mode propagation constant decreases

monotonically in the propagation direction. The difference in modal propagation constant between input and output cross sections of the taper depends on the dimensions of the respective cross sections and on the transverse index contrast. A large core/cladding index contrast can result in a significant decrease in propagation constant and can therefore complicate the choice of the reference propagation constant β_0. At first sight it is not obvious whether this problem appears in the case of the semiconductor tapers under consideration.

If the fundamental mode and radiation modes couple to and fro, the correct propagation of the radiation modes is of importance. If the effective indices of the radiation modes differ too much from that of the fundamental mode, errors may be introduced as the reference index is mainly adapted to the effective index of the fundamental mode. However, the numerical results in Tables III–V have shown that the paraxial methods cope successfully with the taper problem. More extensive simulations of the University of Twente have revealed that the inclusion of the higher order correction terms to the SVEA do not influence the basic result. It can be shown
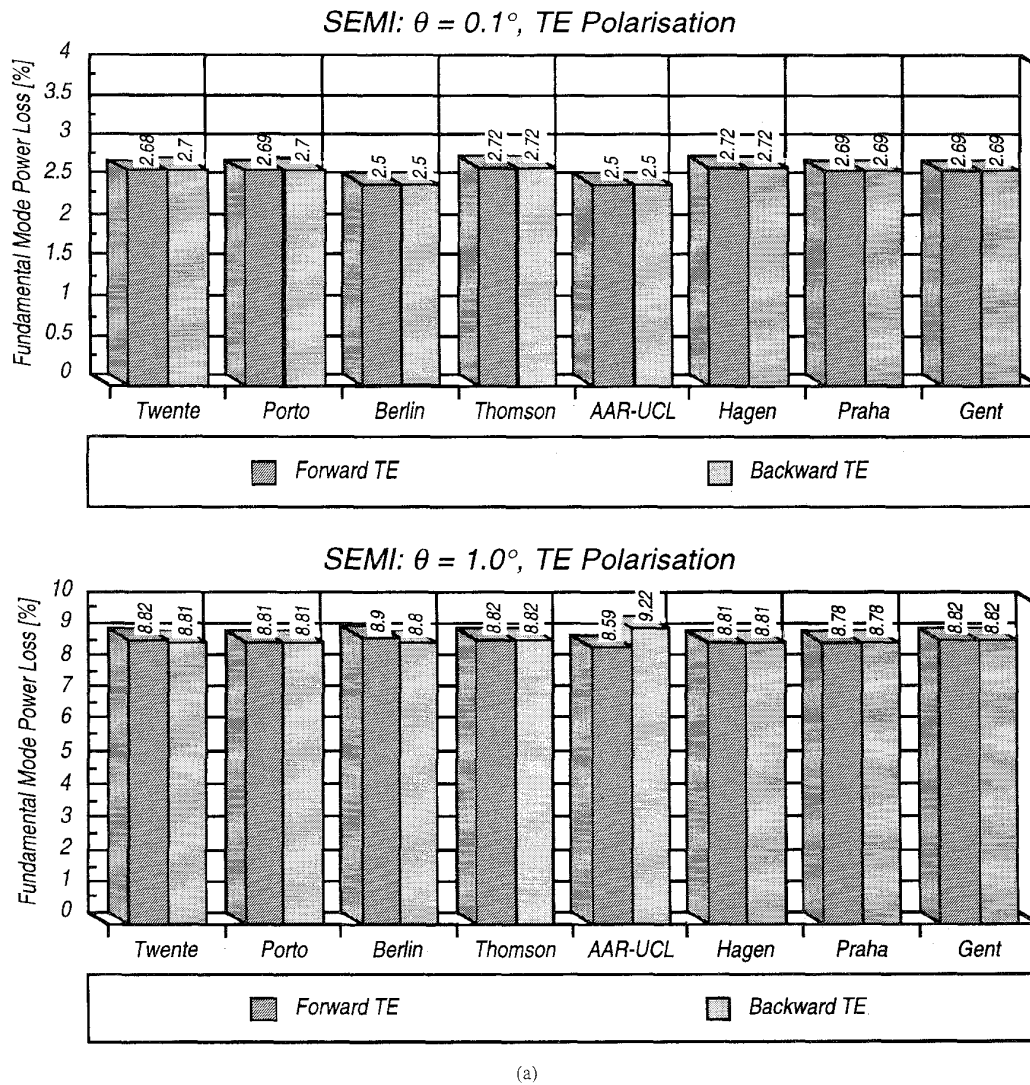
(a)

Fig. 4.   Bar chart representation of the loss figures for the fundamental mode power at the output of the SEMI tapers: (a) TE case

[10] that the error in the propagation constants due to the application of the SVEA are, for the standard FD–BPM

$$\Delta n_{\mathrm{eff}}^{(0)} = \frac{(n_{\mathrm{eff}} - n_0)^2}{2n_0} \tag{2a}$$

where $n_0 = \beta_0/k_0$ stands for the background index and n_{eff} is the correct mode effective index. This assumes that both the step size Δz and the transverse discretization are sufficiently small. The deviation Δn_{eff} reduces including the second order correction terms to

$$\Delta n_{\mathrm{eff}}^{(2)} = -0.06 \frac{(n_{\mathrm{eff}} - n_0)^5}{n_0^4}. \tag{2b}$$

Taking a worst case scenario and putting $n_{\mathrm{eff}} = 3.233\,861$, which is the highest effective index of the exercise occurring at the input section of the AIR taper, and $n_0 = 3.17$, the substrate index, gives $\Delta n_{\mathrm{eff}}^{(0)} = 6.4 \times 10^{-4}$ and $\Delta n_{\mathrm{eff}}^{(2)} = 6.3 \times 10^{-10}$. The deviation $\Delta n_{\mathrm{eff}}^{(0)}$ is indeed small and including the second

order correction should lead to a very accurate solution. The formulas (2) also reveal that good accuracy can be achieved only if the propagation can be well described by one single mode for which n_0 can be chosen close to n_{eff}.

Furthermore, the Thomson BPM does not apply any correction to the propagation constant. Hence, the fundamental mode propagation in typical III-V semiconductor single mode tapers can be described by paraxial formalisms. It might be surprising at first glance that this conclusion still holds for the AIR case. However, since the substrate index again equals 3.17, the variation of the propagation constant of the local fundamental guided mode throughout the taper covers almost the same interval as in the SEMI case.

B. Discretization Effort

Tables III–V give also an indication about the numerical effort for all methods. The transversal discretization N_x and the number of propagation steps N_z, which coincides with the
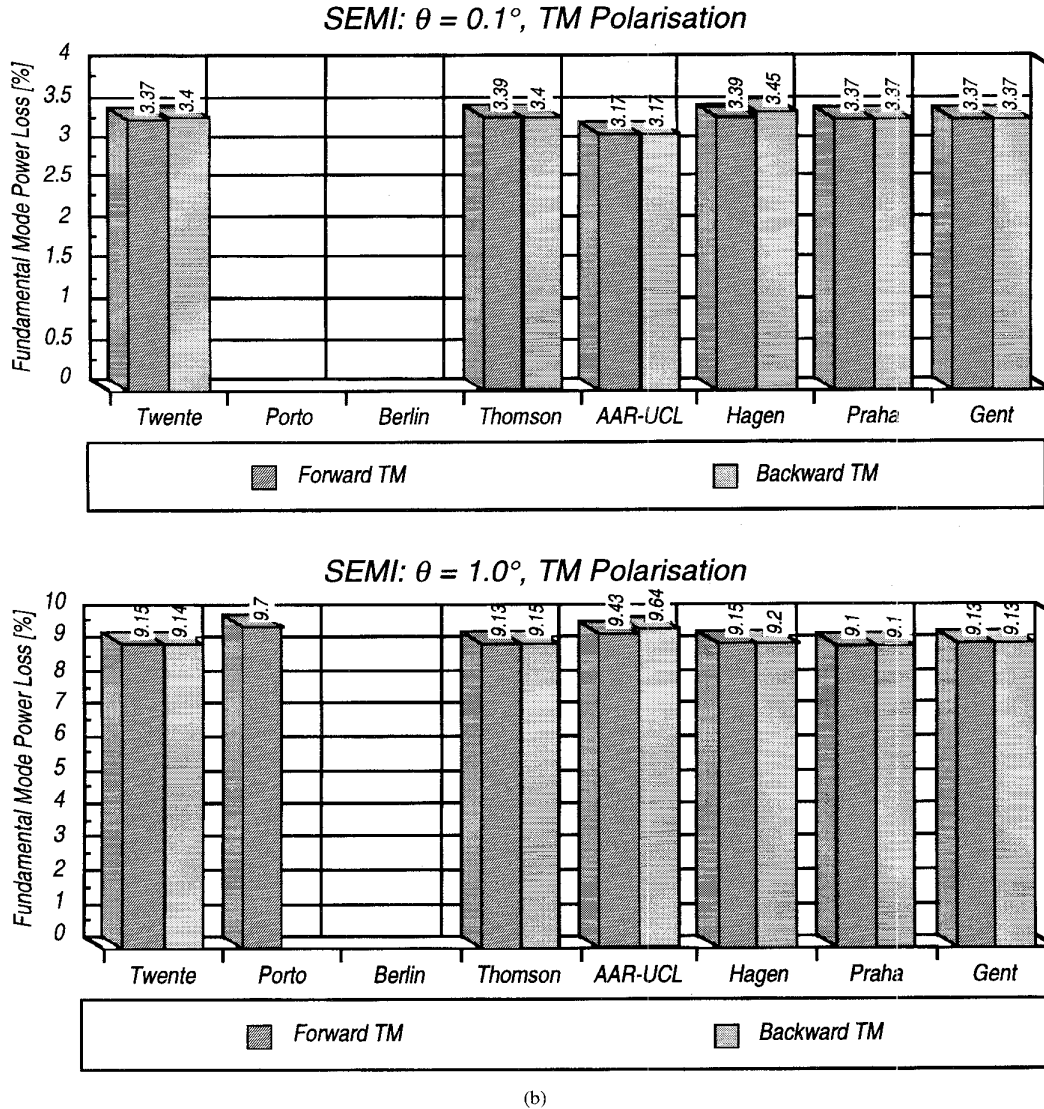
Fig. 4. *(Continued.)* Bar chart representation of the loss figures for the fundamental mode power at the output of the SEMI tapers: (b) TM case.

longitudinal staircase approximation of the tapered waveguide, are listed. In case of the nonparaxial mode expansion techniques N_x stands respectively for the number of modes (IREE and Gent) or for the number of lines. It is apparent that N_z scales with the taper angle for the paraxial algorithms, while the number of propagation steps is generally independent of θ in the nonparaxial cases. Comparing the discretizations of IREE and Gent for the SEMI case it follows that the mode expansion results converge very fast as a function of N_z. This means that a rough discretization of the taper profile approximates well enough the physical wave propagation, provided that the paraxial propagating part of the radiation field is well described. It is also noticed that the algorithms of the Universities of Twente and Porto use a rather large propagation step and a dense transverse discretization, while HHI and Thomson–CSF propagate with very small steps and apply a rougher x discretization. The propagation step

used by AAR-UCL is an order of magnitude larger than the propagation step of the Universities of Twente and Porto.

C. Power Calculation and Reciprocity for Paraxial Propagation

It is well known [12] that the paraxial wave equation does not conserve the longitudinal power flux per surface unit as defined by (Poynting vector)

$$\frac{1}{2}\Re e\left(\int_{-\infty}^{+\infty} \mathbf{E} \times \mathbf{H}^* \cdot \mathbf{u}_z dx\right) \tag{3}$$

but conserves instead the quantity

$$\int_{-\infty}^{+\infty} |\mathbf{E}|^2 dx \tag{4a}$$

TABLE V

SUMMARY OF THE FUNDAMENTAL MODE POWER LOSS VALUES α AS OBTAINED BY THE DIFFERENT PARTICIPANTS FOR THE TE MODE PROPAGATION IN THE AIR TAPERS. AN INDICATION OF THE DISCRETIZATION EFFORT IS ALSO LISTED. IN THE N_X CELL FOR AAR-UCL FIRST THE N_X-FORWARD IS LISTED AND THEN THE N_X-BACKWARD VALUE. THE ASTERISK IN THE MEPM RESULTS DENOTE THAT N_X STANDS FOR THE NUMBER OF THE MODES INSTEAD OF THE TRANSVERSE DISCRETIZATION

| AIR TE	$\theta = 0.1°$ $L = 229$ μm					$\theta = 1.0°$ $L = 22.9$ μm					
	Forward		Backward			Forward		Backward			
	$\alpha(L/2)$ [%]	$\alpha(L)$ [%]	$\alpha(L/2)$ [%]	$\alpha(L)$ [%]	N_z	$\alpha(L/2)$ [%]	$\alpha(L)$ [%]	$\alpha(L/2)$ [%]	$\alpha(L)$ [%]	N_z	N_x
Twente	0.01	3.19	3.29	3.36	400	0.90	17.7	20.9	17.7	400	2048
Porto	0.07	3.30	3.26	3.40	400	0.97	17.8	20.9	17.6	40	2500
HHI	0.00	3.30	3.40	3.50	4241	0.90	18.4	21.6	18.5	424	1024
Thomson	0.03	3.46	3.32	3.39	2290	0.94	17.9	21.0	17.7	229	1024
AAR-UCL	0.07	2.50	2.05	1.83	558	0.92	14.7	17.8	14.3	92	380/390
Hagen	0.02	3.64	3.58	3.64	60	0.92	18.5	21.6	18.6	60	334
IREE[*]	0.03	3.40	3.34	3.40	200	0.90	17.7	20.9	17.7	200	50
Gent[*]	0.09	3.48	3.36	3.48	100	0.95	17.6	20.9	17.6	50	60
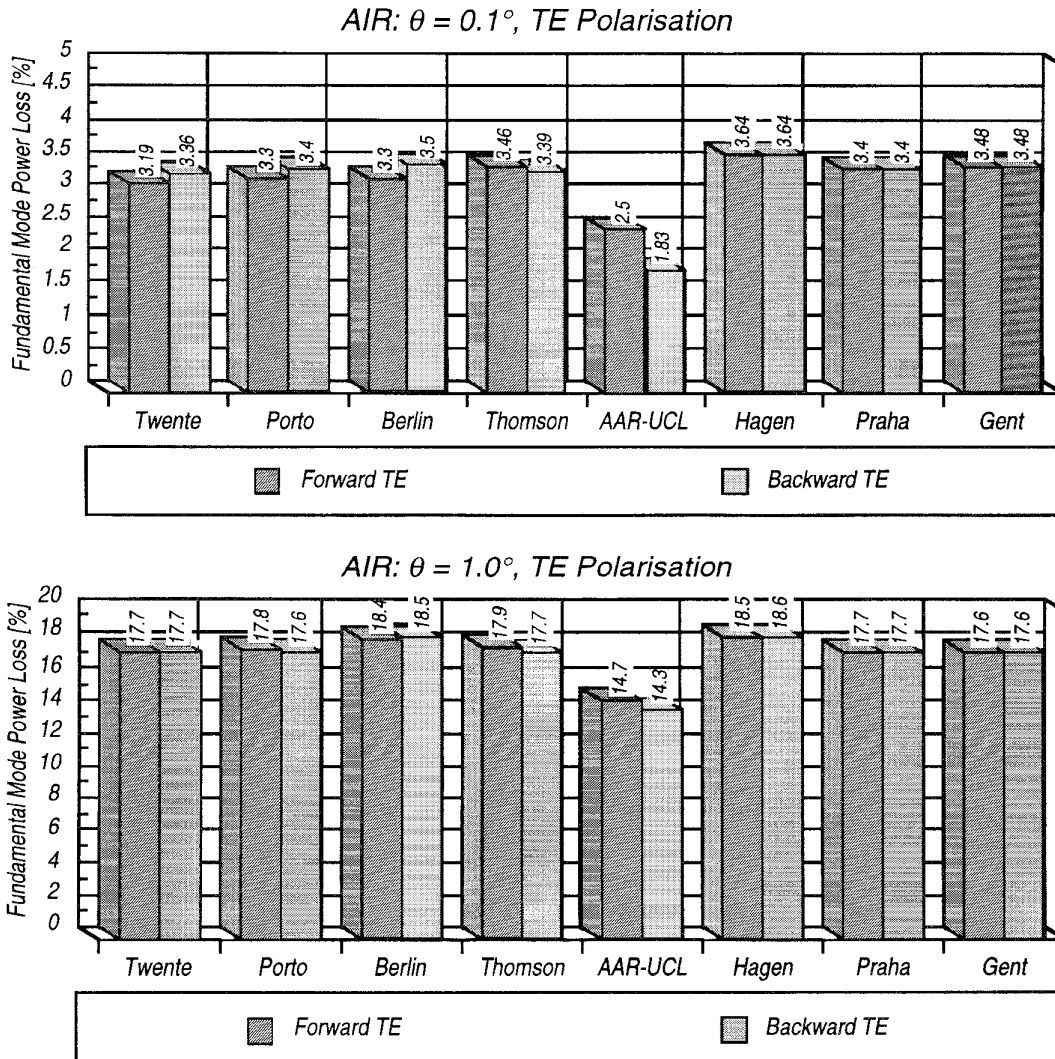
Fig. 5. Bar chart representation of the loss figures for the fundamental mode power at the output of the AIR tapers.
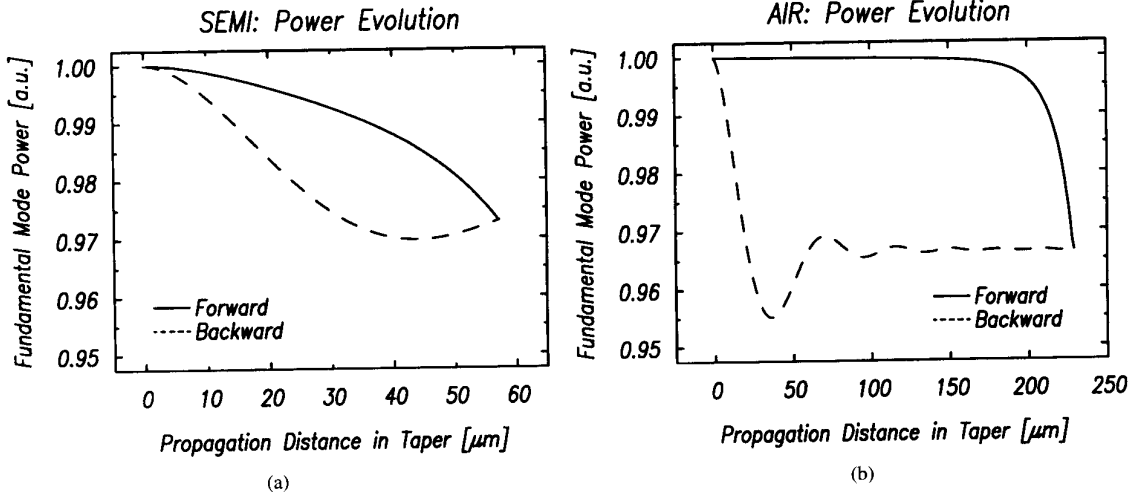
Fig. 6. TE power evolution for the $\theta = 0.1°$ case for the SEMI (a) and AIR (b) tapers. The results were obtained by the Gent-MEPM using 200 propagation steps and 51 modes for the SEMI case and 60 modes for the AIR case.

for TE polarization and

$$\int_{-\infty}^{+\infty} \frac{1}{n^2} |\mathbf{H}|^2 dx \tag{4b}$$

for TM polarization. One should use the integrals (4) to calculate the power content of a propagating field at a certain longitudinal position. Especially, the power transfer between input and output sections has to be calculated using (4), where $|\mathbf{E}|$ and $|\mathbf{H}|$ stand for the magnitude of the local fundamental mode. This is also the case when doing a unidirectional mode expansion propagation [21]. It should be noted that the SVEA, which neglects the second order z derivative in the wave equation, excludes backward propagating waves.

Formula (3) reduces, in case of the propagation of a single TE polarized mode, to

$$\frac{\beta}{2\omega\mu_0} \int_{-\infty}^{+\infty} |\mathbf{E}|^2 dx = \frac{\beta}{2\omega\mu_0} \int_{-\infty}^{+\infty} |E_y|^2 dx \tag{5}$$

where E_y represents the local mode electric field component. Equation (5) is proportional to (4) with the propagation constant as waveguide dependent proportionality factor. Comparison of (4a) with (5) also leads to the insight that (4a) can be considered as a paraxial approximation of (3) or (5) where the variation of the propagation constant β is neglected. Calculating the power transfer from input to output using (5), the ratio between the propagation constants at input and output section is introduced. It follows directly from (5) that

$$\frac{1 - \alpha'(L)_{\text{forward}}}{1 - \alpha'(L)_{\text{backward}}} = \left(\frac{\beta_{z=L}}{\beta_{z=0}}\right)^2 \tag{6}$$

where the prime denotes power calculation using the Poynting vector. Hence the reciprocity criterion cannot be fulfilled if the power transfer is calculated with (3) or (5). The property of reciprocity reduces in this case to the observation that the

ratio of the forward and backward power transfer depends only on the respective waveguide cross sections at input and output and is independent of the connecting waveguide, as expressed mathematically by (6). The ratio (6) in the case of the SEMI taper equals 0.993 as can be readily obtained from the calculated propagation constants at input and output sections.

D. Power Evolution Through the Taper

The power content of the TE fundamental mode as a function of propagation distance calculated by mode expansion is plotted in Fig. 6 for the SEMI and AIR $\theta = 0.1°$ tapers. It is observed that due to the reciprocity of the propagation, the end points of solid and dashed curves coincide. Furthermore, the curves describing the forward propagation show that, especially for the AIR taper, power losses start to increase rapidly for smaller taper thicknesses when the waveguide mode comes close to cut off. This is also suggested by the values of the power losses at half the taper length, see Tables III–V. For a waveguide near cut-off, the mode is guided by a high index region which is very thin compared to the mode size. A small thickness variation will therefore have a dramatic influence on the mode shape and mode width and will imply a considerable radiation loss [4].

The power evolution in the backward AIR case shows an oscillatory behavior. The considerable power loss of the fundamental mode at the beginning of the taper results in a strong coupling between the guided mode and the radiation spectrum. The coupling distance for power exchange from guided mode to radiation modes and back to the guided mode is about 70 μm as can be read from Fig. 6. In Fig. 7 the modulus of the overlap integral between the guided mode at $z = 0$ μm and the radiation modes at $z = 35$ μm is plotted as a function of the effective index of these radiation modes. The overlap integral is taken over the 20 μm wide calculation window (5 μm air cladding). The maximum overlap integral equals 0.18 for an effective radiation mode index of 3.1657 and the centre of the high overlap peak lies around 3.161.
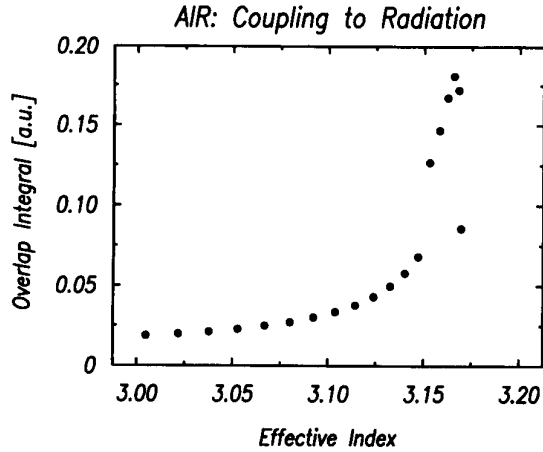
Fig. 7. Coupling between the guided mode and the discretised radiation spectrum for the AIR θ = 0.1° backward case. The modulus of the overlap integral between the guided mode at input and the radiation modes at z = 35 μm is plotted.

The guided mode has an index of 3.1837 which leads to a coupling length of

$$L = \frac{2\pi}{\Delta\beta} = \frac{\lambda}{\Delta n_{eff}} = \frac{1.55\ \mu m}{3.1837 - 3.161} = 68\ \mu m \qquad (7)$$

which corresponds with the observed coupling length on the power plot of Fig. 6.

VI. COMPARISON WITH A FABRICATED TAPER STRUCTURE

Three of the above mentioned two dimensional propagative methods (the HHI FD-BPM and the MEPM of IREE and Gent) were used to calculate the losses of a waveguide taper recently fabricated at the Heinrich Hertz Institute [22]. It consists of a buried rib waveguide (rib width 3 μm, rib height 0.1 μm, film layer thickness at the waveguide port 0.72 μm, λ_q = 1.06 μm material) which is linearly tapered down over a length L, such that at the taper end only a strip waveguide of the width and height of the rib is left (Fig. 8). The mode transformation is stabilised by thin guiding layers above and below the waveguide.

The vertical cross section was represented by the corresponding slab waveguide. The coupling loss to a slab equivalent of a single mode fiber (8.7 μm thick symmetric slab with 1.4650/1.4694 cladding/core index contrast) was calculated and measured. For a taper of length L = 1000 μm the calculations of the different groups yielded 0.6 dB (HHI), 1.6 dB (IREE) and 1.45 dB (Gent). The calculation parameters and the results are summarized in Table VI. The measured loss of the fabricated taper was found to be 1.5 dB and the calculations yielded losses of 0.6 dB (HHI), 1.0 dB (IREE) and 0.85 dB (Gent). Both experimental and calculated losses do not include the Fresnel losses at the interface between taper end facet and fiber. The Fresnel loss can be estimated by the effective indices of the local fundamental modes of the taper output section and the fiber to be 0.6 dB. This reflection loss has been compensated for in the results of the algorithms of IREE and Gent, which include noncoherent reflections. A contour plot of the field propagation is given in Fig. 9.
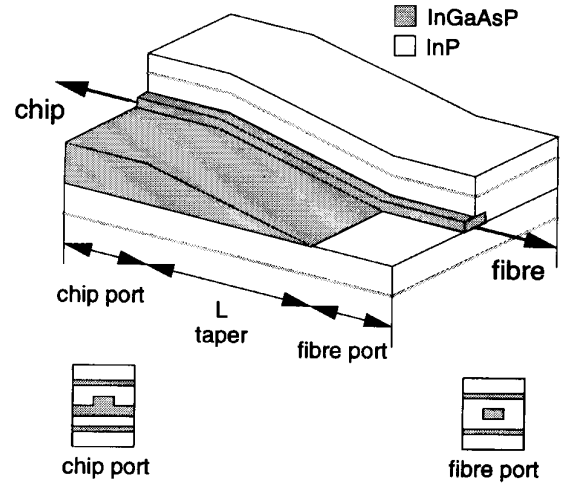

Fig. 8. Schematic view of the experimentally realized taper structure.

TABLE VI
SUMMARY OF THE SINGLE MODE FIBER COUPLING LOSSES OBTAINED BY THE DIFFERENT PARTICIPANTS FOR THE TE MODE PROPAGATION IN THE EXPERIMENTAL TAPER. AN INDICATION OF THE DISCRETIZATION EFFORT IS ALSO LISTED. THE ASTERISK IN THE MEPM RESULTS DENOTE THAT N_X STANDS FOR THE NUMBER OF THE MODES INSTEAD OF THE TRANSVERSE DISCRETIZATION. THE LAST COLUMN MENTIONS THE IMPROVEMENT IN COUPLING EFFICIENCY COMPARED TO THE UNTAPERED DEVICE (CROSS SECTION OF THE CHIP PORT)

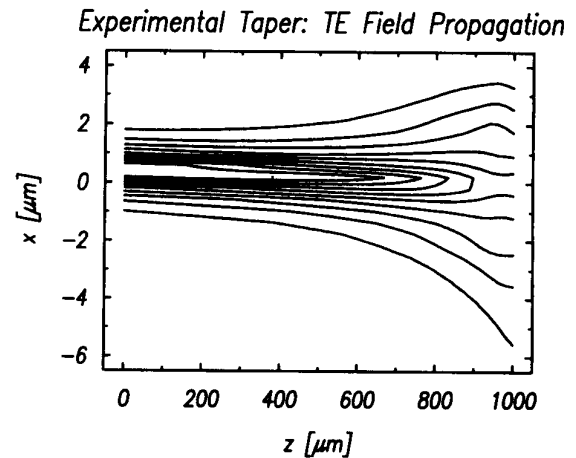|	Coupling loss [dB]	N_z	N_x	Improvement [dB]
HHI	0.6	1000	1024	4.4
IREE*	1.0	52	36	4.0
Gent*	0.85	100	71	4.15
Measurement	1.5			3.8

Fig. 9. Contour plot of the TE field propagation through the experimentally realized taper structure. The plot shows the Gent-MEPM propagation with 100 propagation steps and 71 radiation modes. The z = 0 μm position corresponds to the interface between chip port and taper, as illustrated in Fig. 8.

The coupling loss of the untapered device was measured to be 5.3 dB and was calculated by a simple slab mode overlap calculation to equal 5.0 dB, thus ignoring Fresnel reflection loss. The improvement in coupling efficiency was

therefore measured to be 3.8 dB. The simulated results estimate 4.4 dB (HHI), 4.0 dB (IREE) and 4.15 dB (Gent) for this improvement.

The loss of a waveguide taper is the sum of the loss due to mode transformation and to mode mismatch. Especially the evaluation of mode mismatch needs calculation of the fields in the physical two dimensional cross section so that comparison with the slab taper structure cannot be very accurate. Therefore, simulation of taper structures emphasise the necessity of full three dimensional propagation calculations.

VII. CONCLUSION

In this paper the applicability of different propagative algorithms for the modeling of tapered high contrast step index slab waveguides was assessed. The work has been done in the framework of the European COST 240 project "Techniques of Modeling and Measuring Advanced Photonic Telecommunication Components". Eight different laboratories participated in the modeling exercise.

The different algorithms covered both paraxial and nonparaxial propagation techniques. All paraxial BPM's were implemented using a finite difference based formulation of the scalar Fresnel wave equation. The nonparaxial schemes solved the Helmholtz equation by method of lines BPM or full mode expansion techniques. The numerical results showed that all methods mastered the propagation through the different taper structures and were able to prove numerically the reciprocity of the propagation. It was also verified that the application of high order correction terms to the slowly varying envelope approximation was not needed to improve the accuracy of the paraxial algorithms. The mode expansion methods, which are the natural methods to solve periodic and segmented waveguide problems [23], have proven their usefulness for the simulation of waveguides with continuously varying refractive index profile.

Furthermore, the way the power content of a propagating mode has to be calculated in the case of the paraxial wave equation has been discussed. More in particular, the relation between the choice of power flux expression and its consequences on the principle of reciprocity has been elaborated.

Finally, a comparison has been made between calculated and measured fiber butt coupling loss. One may argue that an absolute comparison between measured and calculated fiber coupling loss, using two dimensional propagation methods, is difficult. Three laboratories participated in the modeling and it turned out that the improvement in coupling efficiency compared to the untapered device could be predicted rather accurately. In the simulations, the fabricated taper was represented by its vertical cross section.

ACKNOWLEDGMENT

REFERENCES

[1] I. Moerman, G. Vermeire, M. D'hondt, W. Vanderbauwhede, J. Blondelle, G. Coudenys, P. Van Daele, and P. Demeester, "III–V semiconductor waveguiding devices using adiabatic tapers," *Microelectron. J.*, vol. 25, pp. 675–690, 1994.

[2] J. D. Love, W. M. Henry, W. J. Stewart, R. J. Black, S. Lacroix, and F. Gonthier, "Tapered single-mode fibers and devices, Part 1: Adiabaticity criteria," *IEE Proc. J.*, 1991, vol. 138, pp. 343–364.

[3] P. G. Suchosky Jr., and V. Ramaswamy, "Exact numerical technique for the analysis of step discontinuities and tapers in optical dielectric waveguides," *J. Opt. Soc. Amer. A*, vol. 3, pp. 194–203, 1986.

[4] J. Haes, J. Willems, and R. Baets, "Design of adiabatic tapers for high contrast step index waveguides," in *Proc. SPIE*, vol. 2212, pp. 685–693.

[5] J. Haes, I. Moerman, P. Demeester, and R. Baets, "Mode expansion simulation of vertical tapers in InP: Comparison with experimental results and optimization," in *Proc. 7th European Conf. Integr. Opt.*, 1995, pp. 399–402.

[6] R. Accornero, M. Artiglia, G. Coppa, P. Di Vita, G. Lapenza, M. Potenza, and P. Ravetto, "Finite difference methods for the analysis of integrated optical waveguides," *Electron. Lett.*, vol. 26, pp. 1959–1960, 1990.

[7] D. Yevick and B. Hermansson, "Split-step finite difference analysis of rib waveguides," *Electron. Lett.*, vol. 25, pp. 461–462, 1989.

[8] R. G. Hadley, "Transparent boundary condition for the BPM," *IEEE J. Quantum Electron.*, vol. 28, pp. 363–370, 1992.

[9] H. J. W. M. Hoekstra, G. J. M. Krijnen, and P. V. Lambeck, "Efficient interface conditions for the finite difference beam propagation method," *J. Lightwav. Technol.*, vol. 10, pp. 1352–1355, 1992.

[10] H. J. W. M. Hoekstra, G. J. M. Krijnen, and P. V. Lambeck, "New formulation of the BPM based on the slowly varying envelope approximation," *Opt. Commun.*, vol. 97, pp. 301–303, 1993.

[11] Y. Chung and N. Dagli, "An assessment of finite difference beam propagation method," *IEEE J. Quantum Electron.*, vol. 26, pp. 1335–1339, 1990.

[12] F. Schmidt, "An adaptive approach to the numerical solution of Fresnel's wave equation," *J. Lightwav. Technol.*, vol. 11, pp. 1425–1434, 1993.

[13] R. D. Ettinger, F. A. Fernandez, J. B. Davies, and H. Bissessur, "Efficient vectorial analysis of propagation in three-dimensional optical devices," in *Proc. Integr. Photon. Res. Topic. Meeting*, 1993, pp. 392–395.

[14] J. Gerdes and R. Pregla, "Beam propagation algorithm based on the method of lines," *J. Opt. Soc. Amer. B*, vol. 8, pp. 389–394, 1991.

[15] R. Pregla and E. Ahlers, "The method of lines for the analysis of discontinuities in optical waveguides," *Electron. Lett.*, vol. 29, pp. 1845–1847, 1993.

[16] S. Helfert and R. Pregla, "Modeling of taper structures in cylindrical coordinates," in *Proc. Integr. Photon. Res. Topic. Meeting*, 1995, pp. 30–32.

[17] S. Helfert and R. Pregla, "New developments of a beam propagation algorithm based on the method of lines," *Opt. Quantum Electron., Special Issue on Optical Waveguide Theory and Numerical Modeling*, vol. 27, no. 10, pp. 943–950, 1995.

[18] G. Sztefka and H. P. Nolting, "Bidirectional eigenmode propagation for large refractive index steps," *IEEE Photon. Technol. Lett.*, vol. 5, pp. 554–557, 1993.

[19] J. Willems, J. Haes, and R. Baets, "The bidirectional mode expansion method for two dimensional waveguides: The TM case," *Opt. Quantum Electron.*, Special Issue on Optical Waveguide Theory and Numerical Modeling, vol. 27, no. 10, pp. 995–1008, 1995.

[20] J. Willems, J. Haes, R. Baets, G. Sztefka, and H. P. Nolting, "Eigenmode propagation analysis of radiation losses in waveguides with discontinuities and grating assisted couplers," in *Proc. Integr. Photon. Res. Topic. Meeting*, 1993, pp. 229–232.

[21] J. Haes, J. Willems, and R. Baets, "Study of power conservation at waveguide discontinuities using the mode expansion method," in *Proc. Integr. Photon. Res. Topic. Meeting*, 1995, pp. 115–117.

[22] L. Moerl, L. Ahlers, P. Albrecht, H. Engel, H. J. Hensel, H. P. Nolting, and F. Reier, "Efficient fiber-chip butt coupling using InGaAsP/InP waveguide tapers," in *Proc. OFC/IOOC*, 1993, pp. 212–213.

[23] H. P. Nolting, R. März, A. D. Capobianco, J. Ctyroky, J. Gerdes, G. R. Hadley, J. Haes, G. J. M. Krijnen, A. Kunz, F. Ladouceur, T. Rasmussen, F. Schmidt, D. Uhlendorf, Ch. Wächter, and L. Leine, "Results of benchmark tests for different numerical BPM algorithms," *J. Lightwave Technol.*, vol. 13, pp. 216–224, 1995.

Jan Haes was born in Gent, Belgium, in 1968. He received the degree in electrical engineering from the University of Gent in 1991. He is currently working toward the Ph.D. degree.

Since September 1991, he has been with the Department of Information Technology of the University of Gent as a research assistent. He holds a research scholarship from the Flemish IWT (Flemish Institute for the promotion of scientific technological research in industry) for doing work in the field of modeling and design of integrated optical waveguides, beam propagation methods, light coupling between waveguides and lasers for optical recording.

Mr. Haes is a member of the Flemish Engineers Association.

Roel Baets (M'88) received the degree in electrical engineering from the University of Gent, Belgium, in 1980. He received the M.Sc. degree in electrical engineering from Stanford University, Stanford, CA, in 1981 and the Ph.D. degree from the University of Gent, Belgium, in 1984.

Since 1981, he has been with the Department of Information Technology of the University of Gent, first as Ph.D. student and later as IMEC-employee in charge of optoelectronic device research. Since 1989 he is a professor in the engineering faculty of the University of Gent. He has worked in the field of III-V devices for optoelectronic systems. He has made contributions to the modeling of semiconductor laser diodes, passive guided wave devices and to the design and fabrication of OEIC's. His main interests now are the modeling, design and testing of optoelectronic devices and systems for optical communication and optical interconnect.

Dr. Baets is a member of the Optical Society of America and the Flemish Engineers Association.

C. M. Weinert, photograph and biography not available at the time of publication.

M. Gravert, photograph and biography not available at the time of publication.

H. P. Nolting, photograph and biography not available at the time of publication.

M. Adelaide Andrade, photograph and biography not available at the time of publication.

A. Leite, photograph and biography not available at the time of publication.

Hans K. Bissessur received the Dipl. Ing. degree from Ecole Polytechnique, France, in 1987, and the Dipl. Ing. and Ph.D. degrees from Ecole Nationale Superieure des Telecommunications in 1989 and 1994, respectively.

In 1989, he joined Alcatel Alsthom Recherche, France, investigating low-linewidth DFB lasers for coherent transmission systems. He was then involved in the development of modeling tools for integrated optics devices and in the design and caracterization of wavelength demultiplexors. He is currently on leave at the Tokyo Institute of Technology, Japan, working on surface-emitting lasers.

J. B. Davies, photograph and biography not available at the time of publication.

Robert D. Ettinger received the B.A. degree in physics from Oxford University in 1981 and the Ph.D. degree in laser theory from Imperial College, University of London, in 1986.

He worked on acousto-optical device modeling at Oxford University Engineering Laboratory and in 1988, he worked on finite element software for integrated optics in the Department of Electronic and Electrical Engineering, University College London. He joined the Department of Computer Science and Information Systems, Brunel University, as lecturer in 1994, with particular interests in automatic problem solving environments and the physics of nonlinear optical waveguides.

Jiri Ctyroky received the university and Ph.D. degrees from the Czech Technical University in Prague in the fields of microwave engineering and laser physics in 1968 and 1972, respectively.

Since then he has been with the Institute of Radio Engineering and Electronics of the Academy of Sciences of the Czech Republic in Prague, working on bulk and guided-wave acousto-optic devices and integrated optics. He received A.v.Humboldt Fellowship for research in integrated optics at the University of Dortmund, Germany. He is also active as a lecturer in Optoelectronics and Guided-wave optics at the Czech Technical University. His main interests are in theory, design, and characterization of optical guided-wave devices.

Dr. Ctyroky is Member of IEEE/LEOS.

E. Ducloux, photograph and biography not available at the time of publication.

F. Ratovelomanana, photograph and biography not available at the time of publication.

N. Vodjdani, photograph and biography not available at the time of publication.

Stefan Helfert was born in Marl, Germany. He received the Master's degree in electrical engineering (Dipl. Ing.) from the Universitaet Dortmund in 1994.

Since 1994, he is with the FernUniversitaet in Hagen, Germany as a Research Assistant. His main research interest is the analysis of integrated optical structures.

Reinhold Pregla (M'76–SM'83) was born in Luisenthal. He received the M.Sc. degree (Dipl.-Ing.) and the Ph.D. degree (Dr.-Ing.) in electrical engineering from the Technische Universitaet Braunschweig, Federal Republic of Germany, in 1963 and 1966, respectively.

From 1966 to 1969, he was a Research Assistant in the Department of Electrical Engineering of the Technische Universitaet Braunschweig (Institut fuer Hochfrequenztechnik), where he was engaged in investigations of microwave filters. After the Habilitation, he was a Lecturer in high frequencies at the Technische Universitaet Braunschweig. Since 1973, he has held the position of Professor at the Ruhr-Universitaet Bochum, Federal Republic of Germany, and since 1975, he has held the position of full Professor in Electrical Engineering at the FernUniversitaet (a university for distance study) in Hagen, Germany. His fields of investigation include microwave and millimeter-wave integrated circuits, field theory, antennas and integrated optics, and photonics.

F. H. G. M. Wijnands, photograph and biography not available at the time of publication.

H. J. W. M. Hoekstra, photograph and biography not available at the time of publication.

G. J. M. Krijnen, photograph and biography not available at the time of publication.